Inorg. Chem. **2007**, *46*, 771–779

New Stannide ScAgSn: Determination of the Superstructure via Two-Dimensional ^{45}Sc Solid State NMR

C. Peter Sebastian,[†] Long Zhang,[‡] Constanze Fehse,[‡] Rolf-Dieter Hoffmann,[†] Hellmut Eckert,*[,‡] and Rainer Pöttgen*[,†]

Institut für Anorganische und Analytische Chemie and NRW Graduate School of Chemistry, Universität Münster, Corrensstrasse 30, D-48149 Münster, Germany, and Institut für Physikalische Chemie and NRW Graduate School of Chemistry, Universität Münster, Corrensstrasse 30, D-48149 Münster, Germany

Received September 7, 2006

The new stannide ScAgSn was synthesized by induction melting of the elements in a sealed tantalum tube and subsequent annealing. ScAgSn crystallizes with a pronounced subcell structure: ZrNiAl type, $P\bar{6}2m$, $a = 708.2(2)$ pm, $c = 433.9(1)$ pm, wR2 = 0.1264, 321 F^2 values, and 14 variables. The Guinier powder pattern reveals weak superstructure reflections pointing to a TiFeSi-type structural arrangement: $I2cm$, $a = 708.1(1)$ pm, $b = 1225.2(2)$ pm, $c = 869.9(1)$ pm, wR2 = 0.0787, 5556 F^2 values, and 49 variables. So far the growth of high-quality single crystals failed. Determination of the superstructure was partly based on merohedral triplet X-ray data augmented by ^{119}Sn Mössbauer spectroscopy and ^{119}Sn and ^{45}Sc solid-state NMR data. In particular, the observation of three crystallographically inequivalent sites in ^{45}Sc NMR triple quantum magic-angle spinning (TQ-MAS) NMR spectra provided unambiguous proof of the superstructure proposed. The ScAgSn structure consists of a three-dimensional [AgSn] network (with Ag–Sn distances between 273 and 280 pm) in which the scandium atoms are located in distorted hexagonal channels, each having five tin and two silver nearest neighbors. Both crystallographically independent tin sites have a tricapped trigonal prismatic coordination, that is, [Sn1Sc$_6$Ag$_3$] and [Sn2Ag$_6$Sc$_3$] environments, which are well distinguished in the ^{119}Sn NMR and Mössbauer spectra because of their different site symmetries.

Introduction

Depending on the size and valence of the rare earth element (lanthanoid contraction), the equiatomic rare earth (RE)-silver-stannides REAgSn adopt different crystal structures. A literature overview was given in a recent paper.[1] With the stable trivalent rare earth elements Y, La−Nd, Sm, and Gd−Er, the REAgSn stannides adopt the hexagonal NdPtSb-type structure, space group $P6_3mc$, a slightly puckered version of AlB_2 with ordered Ag_3Sn_3 hexagons.[2] EuAgSn[3] and YbAgSn[4] with divalent europium and ytterbium have different crystal structures. The europium compound adopts the orthorhombic KHg_2-type structure, space group *Imma*, and YbAgSn crystallizes with the YbAgPb-type, space group $P\bar{6}m2$, with one planar and two puckered Ag_3Sn_3 hexagons. The three structure types derive from the aristotype AlB_2.[2]

With the smaller rare earth elements thulium and lutetium, we observed a switch in structure type.[1] TmAgSn and LuAgSn crystallize with the ZrNiAl structure, a ternary ordered version of the Fe_2P type. The structure of the two stannides could only be solved unambiguously from a combination of diffraction techniques (laboratory and synchrotron X-ray data) and solid-state spectroscopy (^{119}Sn NMR and Mössbauer spectroscopy). The stannides contain two crystallographically independent tin sites in trigonal prismatic coordination.

* To whom correspondence should be addressed. E-mail: eckerth@uni-muenster.de (H.E.); pottgen@uni-muenster.de (R.P.).
[†] Institut für Anorganische und Analytische Chemie.
[‡] Institut für Physikalische Chemie.

(1) Sebastian, C. P.; Eckert, H.; Fehse, C.; Wright, J. P.; Attfield, J. P.; Johrendt, D.; Rayaprol, S.; Hoffmann, R.-D.; Pöttgen, R. *J. Solid State Chem.* **2006**, *179*, 2376−2385.
(2) Hoffmann, R.-D.; Pöttgen, R. *Z. Kristallogr.* **2001**, *216*, 127−145.
(3) Müllmann, R.; Ernet, U.; Mosel, B. D.; Eckert, H.; Kremer, R. K.; Hoffmann, R.-D.; Pöttgen, R. *J. Mater. Chem.* **2001**, *11*, 1133−1140.
(4) Pöttgen, R.; Arpe, P. E.; Felser, C.; Kuβmann, D.; Müllmann, R.; Mosel, B. D.; Künnen, B.; Kotzyba, G. *J. Solid State Chem.* **1999**, *145*, 668−677.

10.1021/ic061691o CCC: $37.00
Published on Web 01/09/2007

Thus, within the REAgSn series, only the representative with scandium was missing. Since scandium has a significantly smaller covalent radius than the smallest rare earth metal lutetium (144 vs 156 pm),[5] either a strong structural distortion or even another structure type is expected. An X-ray powder pattern of our ScAgSn sample revealed additional reflections pointing to a superstructure with small structural distortions. This is the normal way out for many intermetallic scandium compounds, as recently shown for the superstructures of $Sc_3Rh_{1.594}In_4$,[6] Sc_3RhC_4, and Sc_3IrC_4.[7]

In addition to the moderate crystal quality of ScAgSn, the similar scattering power of silver and tin for X-rays (three-electron difference and trilling formation because of a *translationengleiche* symmetry reduction) complicated the structure elucidation. We have therefore used ^{45}Sc high-resolution solid-state NMR as a new spectroscopic tool for structure determination. Even though the ^{45}Sc isotope has excellent NMR receptivity, the moderately large nuclear electric quadrupole moment of this nucleus leads to rather strong quadrupolar perturbations of the NMR signals, often resulting in excessive line broadening effects. As a result, NMR structural studies using the ^{45}Sc isotope have been rather scarce,[8−10] and to the best of our knowledge, no work on intermetallic compounds has been reported so far, aside from our own recent contributions. Our investigations on ScAuSn[11] and ScCuSn[12] clearly showed that well resolved scandium spectra can be obtained, and in the case of ScAuSi,[13] it was possible to distinguish the two crystallographically independent scandium positions. Herein, we report on the structure elucidation of TiFeSi-type[14] ScAgSn by diffraction and spectroscopic techniques. ScAgSn is the first intermetallic scandium compound where two-dimensional ^{45}Sc solid-state NMR has been developed for structure determination, clearly revealing the three crystallographically independent scandium sites.

Experimental Section

Synthesis. The starting materials for the preparation of ScAgSn were a scandium ingot (Kelpin), silver wire (Degussa-Hüls, Ø 1 mm), and tin granules (Merck), all with stated purities better than 99.9%. The three elements were mixed in the ideal 1:1:1 atomic ratio and sealed in tantalum ampules under an argon pressure of about 800 mbar in an arc-melting apparatus.[15] The argon was purified before over titanium sponge (870 K), silica gel, and molecular sieves.

The tantalum ampules were subsequently placed in a water-cooled sample chamber of an induction furnace[16] (Hüttinger Elektronik, Freiburg, Typ TIG 2.5/300), first rapidly heated to ~1500 K and kept at that temperature for 10 min. Finally, the temperature was lowered to 900 K, and the sample was annealed at that temperature for another 4 h, followed by quenching by switching off the power supply. The temperature was controlled through a Sensor Therm Metis MS09 pyrometer with an accuracy of ±30 K. The tantalum tube was subsequently sealed in an evacuated quartz tube for oxidation protection and heated to 923 K in a muffle furnace for 10 days. Finally, the sample was quenched by radiative heat loss outside the furnace. The brittle product could easily be separated from the tantalum tube. No reaction with the container material was observed. The sample is stable in moist air over months. Single crystals exhibit metallic luster.

X-ray Powder Diffraction Data. The ScAgSn sample was characterized through a Guinier powder pattern with α-quartz (a = 491.30 pm, c = 540.46 pm) as an internal standard and Cu Kα_1 radiation. The Guinier camera was equipped with an imaging plate system (Fujifilm, BAS-1800). The stronger reflections of the diagram could easily be indexed on the basis of a small hexagonal unit cell with the lattice parameters a = 708.2(2) pm and c = 432.9(1) pm. However, some weak reflections remained, indicating superstructure formation. The most common superstructure variants of Fe_2P/ZrNiAl are the hexagonal HfRhSn type[17] upon doubling the subcell c axis or the orthorhombic TiFeSi type.[14] Indexing of the powder pattern then succeeded on the basis of a TiFeSi-type cell. To ensure correct indexing, the experimental pattern was compared to a calculated one,[18] taking the positions derived from the single-crystal data. The lattice parameters determined on the single-crystal diffractometer were in good agreement with the powder data. The three strongest superstructure reflections visible on the Guinier pattern were (*hkl*, experimental intensity with respect to the strongest subcell reflection): 321 (5%), 310 (2%), and 132 (2%).

Single-Crystal X-ray Data. Small irregularly shaped crystals of ScAgSn were selected from the crushed arc-melted sample, glued to small quartz fibers using bees wax and then check by Laue photographs on a Buerger camera, equipped with the same Fujifilm, BAS-1800 imaging plate technique. Only a few crystals with sufficient quality for further investigations were found. One crystal was measured at room temperature using a Stoe IPDS-II diffractometer with graphite monochromatized Mo Kα radiation in oscillation mode. The absorption correction was numerical. All relevant crystallographic data for the data collection and evaluation are listed in Table 1.

Scanning Electron Microscopy. The single crystal investigated on the diffractometer and the bulk sample were analyzed using a Leica 420 I scanning electron microscope with Sc, Ag, and Sn as standards. No impurity elements heavier than sodium were observed (detection limit of the machine). The composition determined by EDX (35 ± 2 at. % Sc, 32 ± 2 at. % Ag, 33 ± 2 at. % Sn) is in good agreement with the ideal 1:1:1 composition. The standard deviations quoted express the compositional variations encountered from the measurements taken at various different spots.

^{119}Sn Mössbauer Spectroscopy. A $Ca^{119m}SnO_3$ source was available for the ^{119}Sn Mössbauer spectroscopic investigations. The

(5) Emsley, J. *The Elements*; Oxford University Press: Oxford, U.K., 1999.
(6) Lukachuk, M.; Zaremba, V. I.; Hoffmann, R. D.; Pöttgen, R. *Z. Naturforsch.* **2004**, *59b*, 182−189.
(7) Vogt, C.; Hoffmann, R. D.; Pöttgen, R. *Solid State Sci.* **2005**, *7*, 1003−1009.
(8) Rossini, A. J.; Schurko, R. W. *J. Am. Chem. Soc.* **2006**, *128*, 10391−10402.
(9) Thompson, A. R.; Oldfield, E. *J. Chem. Soc., Chem. Commun.* **1987**, 27−29.
(10) Madhu, P. K.; Johannesson, O. G.; Pike, K. J.; Dupre, R.; Smith, M. E.; Levitt, M. H. *J. Magn. Reson.* **2003**, *163*, 310−317.
(11) Sebastian, C. P.; Eckert, H.; Rayaprol, S.; Hoffmann, R. D.; Pöttgen, R. *Solid State Sci.* **2006**, *8*, 560−566.
(12) Sebastian, C. P.; Eckert, H.; Hoffmann, R. D.; Pöttgen, R. *Solid State Sci.* in press.
(13) Sebastian, C. P.; Eckert, H.; Pöttgen, R. Unpublished results.
(14) Jeitschko, W. *Acta. Crystallogr. B* **1970**, *26*, 815−822.
(15) Pöttgen, R.; Gulden, Th.; Simon, A. *GIT Labor-Fachz.* **1999**, *43*, 133−136.
(16) Kuβmann, D.; Hoffmann, R. D.; Pöttgen, R. *Z. Anorg. Allg. Chem.* **1998**, *624*, 1727−1735.
(17) Zumdick, M. F.; Pöttgen, R. *Z. Kristallogr.* **1999**, *214*, 90−97.
(18) Yvon, K.; Jeitschko, W.; Parthé, E. *J. Appl. Crystallogr.* **1977**, *10*, 73−74.

Table 1. Crystal Data and Structure Refinement for ScAgSn

	subcell	superstructure
empirical formula	ScAgSn	
molar mass	271.52 g/mol	
unit cell dimensions (Guinier powder data)	$a = 708.2(2)$ pm $b = a$ $c = 433.9(1)$ pm $V = 0.1885$ nm^3	$a = 708.1(1)$ pm $b = 1225.2(2)$ pm $c = 869.9(1)$ pm $V = 0.7547$ nm^3
space group	$P\bar{6}2m$	$I2cm$[a]
structure type	ZrNiAl	TiFeSi
Pearson symbol	hP9	oI36
formula units	$Z = 3$	$Z = 12$
calculated density	7.18 g/cm^3	
crystal size	$45 \times 65 \times 90$ μm^3	
transmission ratio (max/min)	1.36	
absorption coefficient	19.8 mm^{-1}	
$F(000)$	354	1416
θ range	3−35°	2−35°
range in *hkl*	−5/+11, ±11, −5/+6	±11, −19/16, −11/12
total reflections	1938	5556
independent reflections	321 ($R_{int} = 0.1283$)	5556 (not merged)
reflections with $I > 2\sigma(I)$	315 ($R_s = 0.0635$)	4722 ($R_s = 0.0442$)
data/parameters	321/14	5556/49
GOF on F^2	1.332	1.022
final R indices	R1 = 0.0569	R1 = 0.0371
[$I > 2\sigma(I)$]	wR2 = 0.1260	wR2 = 0.0739
R indices	R1 = 0.0578	R1 = 0.0477
(all data)	wR2 = 0.1264	wR2 = 0.0787
BASF		0.507(1)[b]
Flack parameter	0.1(5)	0.03(7)
extinction coefficient	0.037(6)	0.0041(2)
largest diff. peak and hole	3.03/ −2.80 e/Å^3	4.25/ −3.44 e/Å^3

[a] *I2cm* is a nonstandard setting of *Ima2*; transformation from *I2cm* to *Ima2* via 0 0 1, 0 −1 0, 1 0 0; new coordinates are *z*, −*y*, *x*. [b] Scale factor for two domains.

sample was placed within a thin-walled PVC container at a thickness that corresponds to a tin surface density of about 10 mg Sn/cm^2. A palladium foil of 0.05 mm thickness was used to reduce the tin K X-ray background concurrently emitted by this source. The measurement was conducted in the usual transmission geometry at $T = 78$ K. The spectra were fitted to Lorentzian doublets, arising from nuclear electric quadrupolar splitting. Appropriate starting values for these fits were quantum-chemical calculations of the electric field gradients using the WIEN2k program code.[19]

^{119}Sn Solid-State NMR. ^{119}Sn NMR spectra were recorded at 149.1 MHz, on a Bruker DSX 400 spectrometer equipped with a 4 mm MAS NMR probe. Spectra were taken on samples spinning at a rate of 10 kHz, using 90° pulses of 2.5 μs for ScAgSn, followed by a relaxation delay of 1 s. Additional measurements were taken at a spinning frequency of 25 kHz using a 2.5 mm MAS NMR probe. Resonance shifts are reported relative to tetramethyltin, using tin(IV) oxide as a secondary reference. To minimize undesirable effects of probe detuning and sample heating of these highly metallic samples, the finely ground powders were mixed with silica in a 1:1 mass ratio. The MAS sideband patterns were fitted, using the DMFIT routine, to yield the anisotropic shielding tensor components with the definitions

$$\delta_{CS} = -(\sigma_{ZZ}^{PAS} - \sigma_{iso})$$

$$\eta_{CS} = \frac{\sigma_{YY}^{PAS} - \sigma_{XX}^{PAS}}{\sigma_{ZZ}^{PAS} - \sigma_{iso}}$$

$$\sigma_{iso} = \frac{1}{3}(\sigma_{XX}^{PAS} + \sigma_{YY}^{PAS} + \sigma_{ZZ}^{PAS})$$

where the superscript PAS refers to the principal axis system of the shielding tensor.

^{45}Sc Solid-State NMR. ^{45}Sc MAS NMR spectra were recorded at ambient temperature at resonance frequencies of 121.5 MHz on a Bruker DSX-500 spectrometer, operating a 2.5 mm MAS NMR probe at a MAS rotation frequency of 25 kHz. Typical pulse lengths of 0.5 μs (20° solid flip angle) were used with a recycle delay of 0.5 s and 2000 scans. The ^{45}Sc NMR shifts are referenced to 0.2 M scandium nitrate aqueous solution. The ^{45}Sc ($I = 7/2$) resonance shifts are influenced by an isotropic Zeeman (magnetic shielding) contribution, δ_{iso}, and a (negative) shift contribution, δ_Q, arising from second-order quadrupolar perturbations. Both effects can be separated using the two-dimensional triple-quantum (TQ)-MAS experiment,[20−22] so that the magnetic shielding contribution, δ_{iso}, can be determined. These TQMAS studies were conducted using the three-pulse zero-quantum filtering variant[21,22] at spinning speeds of 25 kHz. The rf field strengths of the first two hard pulses (lengths 1.8 μs and 0.6 μs, respectively) and the third soft pulse (5.0 μs length) corresponded to nutation frequencies of approximately 80 and 10 kHz, respectively for a liquid sample. Nine hundred sixty transients were accumulated for each t_1 increment, and a total of 300 increments were done at steps of 5 μs. The sheared spectra were analyzed by projecting the 2D contour plots for each individual site onto the F_1 and F_2 axes.[21,22]

Theoretical Calculations. To aid the site assignments to the NMR signals, the program WIEN2k was used for DFT calculations of the electric field gradients V_{ii} for the various Sn and Sc atomic positions. This program package is a full-potential all-electron method based on the LAPW +LO method. For the calculations on a single computer, the following atomic-sphere radii, defined as R_{MT}- values (R_{MT}), and given in atomic units, are recommended to obtain non-overlapping spheres and an advantageous matrix size defined by the product $R_{MT}K_{Max}$: Sc (1.7), Ag (1.8), and Sn (1.9). A separation energy of −7.0 Ry is used to separate the core states from the valence states and to avoid the so-called core-charge leakage. In this way, the 4s orbitals of tin are included in the core states. For describing the first Brillouin zone, we used 30 k-points; this is increased up to 50 k-points in 10-steps in all calculations. About 3000 plane waves were necessary to describe the electronic state of the crystal system.

Results and Discussion

Structure Refinement. In the first refinement step, all weak superstructure reflections have been neglected, and only the subcell intensities have been integrated. Since isotypy with TmAgSn and LuAgSn[1] (ZrNiAl type, space group $P\bar{6}2m$) was already evident from the X-ray powder data, the atomic parameters of LuAgSn were taken as starting values,

(19) Blaha, P.; Schwarz, K.; Madsen, G. K. H.; Kvasnicka, D.; Luitz, J. *WIEN2k, An Augmented Plane Wave + Local Orbitals Program for Calculating Crystal Properties*; Karlheinz Schwarz Technical Universität: Wien, Austria, 2001; ISBN 3-9501031-2.

(20) Medek, A.; Harwood, J. S.; Frydman, L. *J. Am. Chem. Soc.* **1995**, *117*, 12779−12787.

(21) Amoureux, J. P.; Fernandez, C.; Steuernagel, S. *J. Magn. Reson.* **1996**, *A123*, 116−118.

(22) Züchner, L.; Chan, J. C. C.; Müller-Warmuth, W.; Eckert, H. *J. Phys. Chem. B* **1998**, *120*, 4495−4506.

Table 2. Atomic Coordinates and Anisotropic Displacement Parameters (pm^2) for the Subcell and the Superstructure of ScAgSn[a]

atom	Wyckoff position	x	y	z	U_{11}	U_{22}	U_{33}	U_{12}	U_{13}	U_{23}	U_{eq}
				subcell, $P\bar{6}2m$							
Sc	3*g*	0.5618(9)	0	1/2	221(20)	56(20)	66(23)	28(10)	0	0	133(10)
Ag	3*f*	0.2434(3)	0	0	90(6)	136(10)	566(18)	68(5)	0	0	259(7)
Sn1	2*c*	2/3	1/3	0	77(5)	U_{11}	79(8)	38(3)	0	0	77(4)
Sn2	1*b*	0	0	1/2	725(28)	U_{11}	97(22)	362(14)	0	0	515(17)
				superstructure, *I*2*cm*							
Sc1	4*b*	0.4577(2)	0.00158(10)	1/4	169(5)	80(4)	54(6)	−9(4)	0	0	101(2)
Sc2	4*b*	−0.18838(19)	−0.20886(11)	1/4	85(5)	133(5)	50(7)	4(4)	0	0	89(2)
Sc3	4*b*	−0.21170(19)	−0.22937(10)	3/4	97(6)	137(6)	67(7)	29(5)	0	0	101(3)
Ag1	4*a*	0.77738(7)	0	0	84(2)	129(2)	266(4)	0	0	13(2)	160(1)
Ag2	8*c*	−0.35628(5)	−0.37900(3)	0.02282(5)	111(1)	90(1)	235(2)	−19(1)	9(2)	0(12)	145(1)
Sn1	8*c*	0.52035(4)	0.16700(2)	−0.00308(4)	87(1)	74(1)	61(1)	−2(1)	1(1)	−1(1)	74(1)
Sn2	4*b*	0.02132(12)	0.02190(4)	1/4	259(2)	198(2)	82(3)	14(3)	0	0	179(1)

[a] U_{eq} is defined as one-third of the trace of the orthogonalized U_{ij} tensor. Special condition for the subcell: $U_{13} = U_{23} = 0$.

Table 3. Interatomic Distances (pm), Calculated with the Lattice Parameters Taken from X-ray Powder Data in the Superstructure of ScAgSn[a]

Sc1	2	Sn1	301.3	Sn1	1	Ag2	273.1	Ag1	2	Sn1	273.9
	2	Sn1	302.5		1	Ag1	273.9		2	Sn2	279.0
	1	Sn2	310.0		1	Ag2	274.6		2	Ag2	299.4
	2	Ag1	313.9		1	Sc3	300.5		2	Sc1	313.9
	2	Ag2	333.2		1	Sc1	301.3		2	Sc2	336.7
	1	Sc3	350.8		1	Sc2	301.9		2	Sc3	355.4
	2	Ag2	356.6		1	Sc2	302.2	Ag2	1	Sn1	273.1
	1	Sc2	359.6		1	Sc1	302.5		1	Sn1	274.6
	1	Sc3	364.3		1	Sc3	302.6		1	Sn2	277.9
	1	Sc2	373.3	Sn2	2	Ag2	277.9		1	Sn2	280.3
Sc2	2	Sn1	301.9		2	Ag1	279.0		1	Ag2	299.1
	2	Sn1	302.2		2	Ag2	280.3		1	Ag1	299.4
	2	Ag2	310.9		1	Sc3	303.0		1	Sc2	310.9
	1	Sn2	319.4		1	Sc1	310.0		1	Sc3	316.9
	2	Ag2	325.5		1	Sc2	319.4		1	Sc2	325.5
	2	Ag1	336.7		1	Sc3	358.6		1	Sc1	333.2
	1	Sc1	359.6						1	Sc1	356.6
	2	Sc2	368.1								
	1	Sc1	373.3								
Sc3	2	Sn1	300.5								
	2	Sn1	302.6								
	1	Sn2	303.0								
	2	Ag2	316.9								
	1	Sc1	350.8								
	2	Ag1	355.4								
	2	Sc3	357.6								
	1	Sn2	358.6								
	1	Sc1	364.3								

[a] All distances within the first coordination spheres are listed. Standard deviations are equal or less than 0.2 pm.

and the structure was refined with anisotropic displacement parameters for all atoms with SHELXL-97 (full-matrix least-squares on F_o^2).[23] Refinement of the correct absolute structure was ensured through refinement of the Flack parameter.[24,25] The refinement converged to the residuals listed in Table 1 and the atomic parameters and interatomic distances given in Tables 2 and 3. The silver−tin ordering on the three sites 3*f*, 2*c*, and 1*b* was checked through refinement of the occupancy parameters, and we observed the same ordering pattern as for TmAgSn and LuAgSn.[1] All sites were fully occupied within two standard uncertainties.

The weak superstructure reflections have been considered in the second step. The additional reflections suggested doubling of all three lattice parameters. Systematic extinctions, not belonging to any space group, however, pointed toward twinning. As a matter of fact, the formation of triplets was found in this case. Since the doubling of the lattice parameters *a* and *b* can be accounted for (and simulated on the basis of) by the twinning effect, only the *c* parameter is doubled in the superstructure. In the diffractometer data of all three domains were collected. This was done using the pseudocell with 2*a*, 2*b*, and 2*c* of the subcell. The data were numerically corrected for absorption using point group 6/*m* to simulate the triplet; only medium strong reflections were considered for the shape refinement using Xshape supplied by Stoe&Cie. The data were sorted with the aid of Hklsort[26] to assign batch numbers and obtain a data file suitable for the hklF5 (forcing no data merging) refinement with SHELXL-97. Detailed analyses of the data revealed that only two domains had considerable scattering intensities. The third domain actually introduced a bias into the refinement and was therefore neglected, even though a small scaling error concerning the fully superimposed subcell reflections was introduced by this procedure.

Data on the structure refinements are available. [Details may be obtained from Fachinformationszentrum Karlsruhe, D-76344 Eggenstein-Leopoldshafen, Germany, by quoting the Registry No. CSD-416974 (superstructure).] The TiFeSi type structure model, space group *I*2*cm* could be refined; however, owing to the many weak reflections and triplet formation the quality of the refinement did not satisfy criteria of a high-quality structure refinement despite the low R-values. Especially some anisotropic displacement parameters still showed some correlation due to the partly merohedral twinning. Also it cannot be ruled out that some of the domains in addition are twinned by inversion (anomalous dispersion is not significant for silver and tin using Mo Kα radiation). The latter will be addressed by near edge X-ray data from a synchrotron source in the future, and attempts for the synthesis of better quality single crystals are under way. Our further discussion is thus augmented by

(23) Sheldrick, G. M. *SHELXL-97, Program for Crystal Structure Refinement;* University of Göttingen: Göttingen, Germany, 1997.
(24) Flack, H. D.; Bernadinelli, G. *Acta Crystallogr. A* **1999**, *55*, 908−915.
(25) Flack, H. D.; Bernadinelli, G. *J. Appl. Crystallogr.* **2000**, *33*, 1143−1148.
(26) Hoffmann, R. D.; Riecken, J. *HKLSORT, Program to Assign Batch Numbers to Various Classes of Reflections;* Universität Münster: Münster, Germany, 2005.

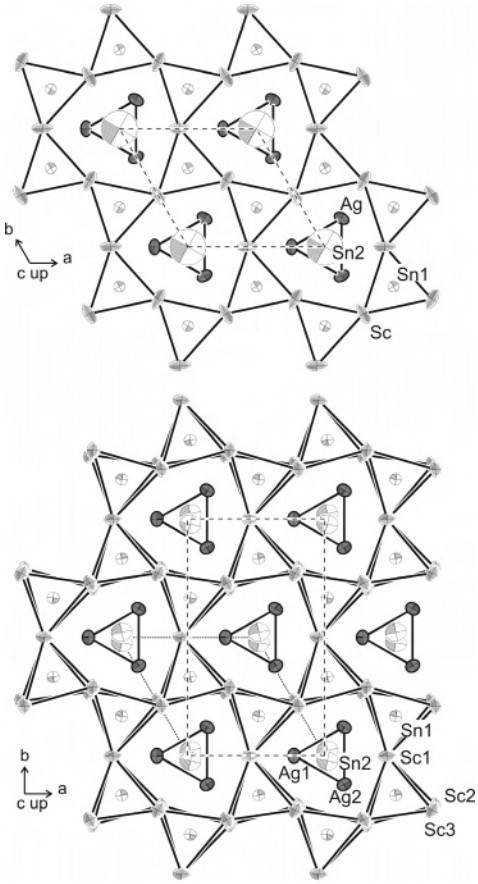

Figure 1. Projection of the ScAgSn substructure (top) and the superstructure (bottom) onto the *xy* planes. Scandium, silver, and tin atoms are drawn as light gray medium gray, and open circles, respectively. In the subcell atoms lie on mirror planes at $z = 0$ (thin lines) and $z = 1/2$ (thick lines). The trigonal prismatic coordination of the two crystallographically independent tin sites is emphasized. The displacement ellipsoids are drawn at the 99% probability level. The unit cell of the substructure is also given by dotted lines in the bottom drawing.

^{45}Sc and ^{119}Sn solid-state NMR spectroscopic data discussed below. The diffraction results are fully supported by the spectroscopy.

Crystal Chemistry. The new stannide ScAgSn adopts a pronounced ZrNiAl type,[27 and ref therein] subcell structure of which has been refined on the basis of single-crystal diffractometer data. A projection of the ScAgSn structure onto the *xy* plane is presented at the top of Figure 1. Both crystallographically independent tin sites have tricapped trigonal prismatic coordination, that is, [Sn1Sc_6Ag_3] and [Sn2Ag_6Sc_3] (Figure 2 top). The shortest interatomic distances occur for the Ag−Sn contacts (273−280 pm), which are close to the sum of the covalent radii of 274 pm.[5] In isotypic TmAgSn (280−284 pm) and LuAgSn (279−284 pm),[1] the Ag−Sn distances are slightly larger, accounting for the larger sizes of thulium and lutetium atoms. The triangular sites of the Ag_6 prisms have an edge length of 299 pm, only slightly longer than the Ag−Ag distances in *fcc* silver.[28] In good agreement with the electronic structure

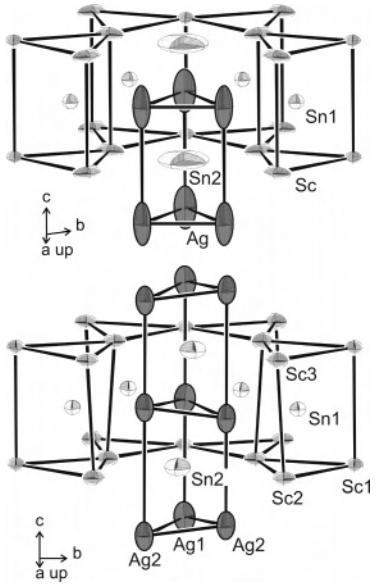

Figure 2. Cutouts of the ScAgSn substructure (top) and the superstructure (bottom). Scandium, silver, and tin atoms are drawn as light gray, medium gray, and open circles, respectively. The trigonal prisms around the tin atoms (Sn2 in the Ag prisms and Sn1 in the Sc prisms) are emphasized. The displacement ellipsoids are drawn at the 99% probability level.

calculations recently performed for LuAgSn,[1] we can safely assume significant Ag−Sn and Ag−Ag bonding interactions for ScAgSn. Since the crystal chemistry of ZrNiAl-type intermetallics has been discussed previously,[17,27,29] we refer to these articles for further information. In the following discussion, we focus on the superstructure formation (Figure 1 bottom).

The different superstructure variants of the Fe_2P/ZrNiAl-type structure have been summarized in refs 6, 17, 29, and 30. Their occurrence arises from small atomic size differences. The size mismatch prevents the high-symmetry structure from being retained, while satisfying bond criteria. Sometimes a change in composition is another way out via site occupancy variations, that is, the $Lu_3Co_2In_4$[31] or $Ti_4Ni_2Ga_3$[32] types. The most common superstructure for the ZrNiAl-related compounds with equiatomic composition is the HfRhSn type,[17] also observed for ScPtSn.[33] In this superstructure variant, the platinum atoms fill the trigonal prisms, while in the case of ScAgSn, these sites are filled by tin. Thus, we observe an exchange of the transition metal and p element positions. In addition, a further distortion is present reducing the space group symmetry from hexagonal to orthorhombic (bottom of Figures 1 and 2).

In the ScPtSn structure, the platinum atoms within the scandium-based prisms dislocate from the subcell mirror

(27) Zumdick, M. F.; Hoffmann, R. D.; Pöttgen, R. *Z. Naturforsch.* **1999**, *54*, 45−53.
(28) Donohue, J. *The Structures of the Elements*; Wiley: New York, 1974.
(29) Parthé, E.; Gelato, L.; Chabot, B.; Penzo, M.; Cenzual, K.; Gladyshevskii, R. E. TYPIX−Standardized Data and Crystal Chemical Characterization of Inorganic Structure Types. In *Gmelin Handbook of Inorganic and Organometallic Chemistry*, 8th ed.; Springer: Weinheim, Germany, 1993.
(30) Bärnighausen, H. *Commun. Math. Chem.* **1980**, *9*, 139−175.
(31) Zaremba, V. I.; Kalychak, Ya. M.; Zavalii, P. Yu.; Sobolev, A. N. *Dopov. Akad. Nauk. Ukr. RSR, Ser. B* **1989**, 38−40.
(32) Markiv, V. Ja.; Beljavina, N. N.; L'isenko, A. A.; Babenko, A. A. *Dopov. Akad. Nauk. Ukr. RSR, Ser. B* **1983**, 34−37.
(33) Mishra, R.; Pöttgen, R.; Hoffmann, R. D.; Trill, H.; Mosel, B. D.; Piotrowski, H.; Zumdick, M. F. *Z. Naturforsch.* **2001**, *56b*, 589−597.

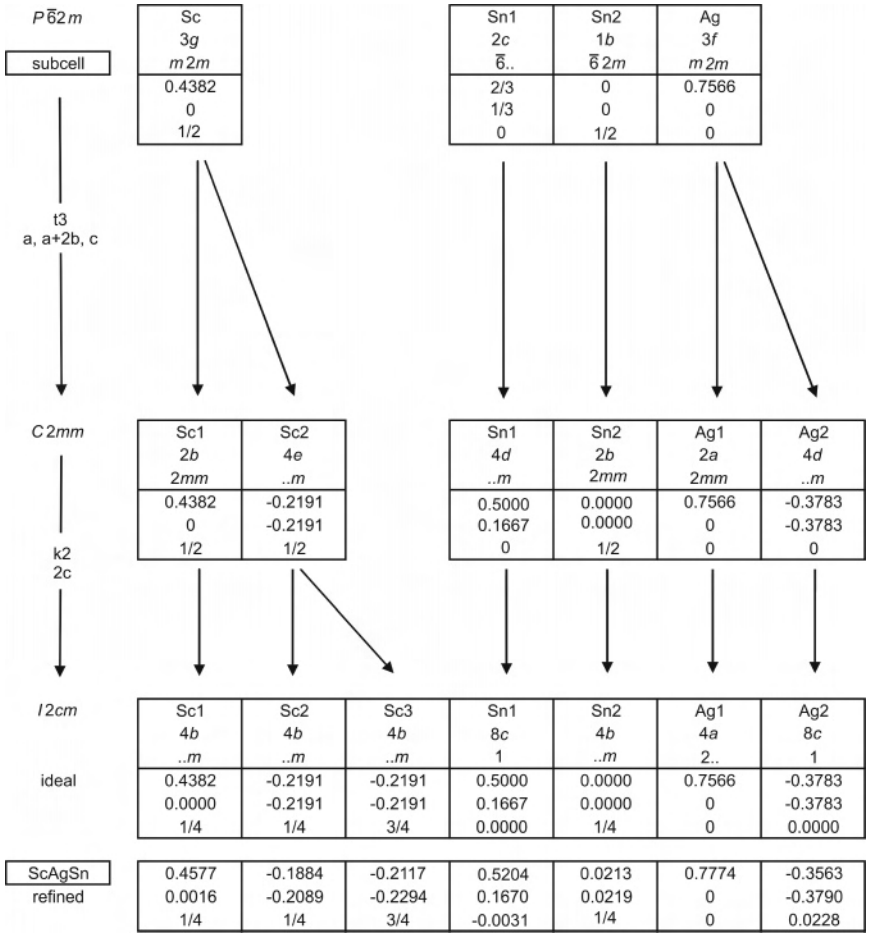

Figure 3. Group−subgroup scheme in the Bärnighausen formalism[30,35,36] for the subcell and the superstructure of ScAgSn. The indices for the *translationengleiche* (t) and *klassengleiche* (k) transitions and the unit cell transformations are given. The evolution of the atomic parameters is shown at the right.

plane at $z = 1/2$. An ordering within the six-membered ring of trigonal Sc_6 prisms can be achieved through a 3 + 3 ordering, and the hexagonal symmetry can be preserved. This ordering pattern is not possible for ScAgSn reported herein. The Sn1 atoms within the Sc_6 prisms show an almost isotropic displacement, while the Sn2 atoms strongly dislocate in the *ab* plane and the Ag atoms within the *c* direction. An ordering model for this type of dislocation is only possible upon enlarging the unit cell at least within the *ab* plane to avoid a frustration. Such an arrangement was first observed for TiFeSi,[14] and today more than 30 intermetallic compounds with this structure type are known.[34]

TiFeSi crystallizes with space group *I*2*cm* (nonstandard setting of *Ima*2). The peculiar displacement parameters refined for the subcell (top of Figures 1 and 2) are resolved in the superstructure (bottom of Figures 1 and 2). Whereas the scandium and Sn1 atoms mainly show dislocations within the *ab* plane, the silver atoms displace along the *c* axis. As shown in the corresponding Bärnighausen tree[35,36] in Figure 3, the symmetry reduction first proceeds via a *translationengleiche* transition of index 3 (t3) from P$\bar{6}$2*m* to *C*2*mm* followed by a *klassengleiche* transition of index 2 (k2) upon doubling the unit cell. In the superstructure, one observes three crystallographically independent scandium sites in the ratio Sc1/Sc2/Sc3 = 1:1:1 (while only one scandium site occurs in the HfRhSn type model for ScPtSn). The *translationengleiche* transition in the first step of the symmetry reduction can cause the formation of triplets, and this was indeed observed for the investigated single crystal. Figure 3 also contains the ideal subcell atomic positions calculated from the average subcell. The various dislocations from the subcell positions nicely reflect the resolution of the anisotropic displacement parameters refined for the subcell. The site assignments are conclusive because the R1 value increases by 0.01 for exchanged Ag/Sn assignments. Thus, there is, in our opinion, no doubt about the correctness of the superstructure model, but the data still contain some bias. Our further discussion is therefore supported by ^{119}Sn and, especially, ^{45}Sc solid-state NMR spectroscopic data.

^{119}Sn Mössbauer Spectroscopy. Figure 4 summarizes the ^{119}Sn Mössbauer spectra of the compound under study. The hyperfine parameters extracted from these data by least-squares fitting are summarized in Table 4. It also includes the theoretical values of the ^{119}Sn quadrupole splitting

(34) Villars, P.; Calvert, L. D. *Pearson's Handbook of Crystallographic Data for Intermetallic Phases*, 2nd ed.; American Society for Metals: Materials Park, OH, 1991 and 1997 (desk edition).
(35) Bärnighausen, H.; Müller, U. *Symmetriebeziehungen zwischen den Raumgruppen als Hilfsmittel zur straffen Darstellung von Strukturzusammenhängen in der Kristallchemie*; University of Karlsruhe and University/GH Kassel: Karlsruhe, Germany, 1996.
(36) Müller, U. *Z. Anorg. Allg. Chem.* **2004**, *630*, 1519−1537.

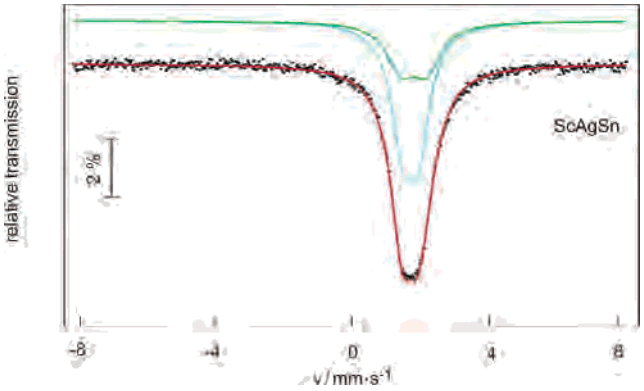

Figure 4. Experimental and simulated ^{119}Sn Mössbauer spectrum of ScAgSn at 78 K.

Table 4. Fitting Parameters of ^{119}Sn Mössbauer Measurements for ScAgSn[a]

δ1	ΔE_{Q1}	Γ1	δ2	ΔE_{Q2}	Γ2	area ratio Sn1/Sn2
1.75(2)	0.45(1) (0.22)	0.71(4)	1.87(2)	0.64(7) (0.68)	1.02(1)	65:35

[a] Numbers in parentheses represent the statistical errors in the last digit. Abbreviations: δ, isomer shift (vs $BaSnO_3$); ΔE_Q, electric quadrupole splitting; Γ, experimental line width. All the parameters are in mm/s. The parameters in parentheses are the quadrupole splittings calculated from the crystal structure via the Wien2k program.

parameter, calculated by the equation

$$\Delta E_Q = eQV_{zz}(1 + \eta^2/3)^{1/2}/2h$$

using the known nuclear electric quadrupole moment (0.128×10^{-28} m^2)[37] of the excited nuclear state ($I = 3/2$), the principal value of the electric field gradient tensor V_{zz} and the asymmetry parameter η as calculated from the WIEN2k program[19] (in the present case, the calculated η values are 0.15 and 0.02 for Sn1 and Sn2, respectively). The resulting value in megahertz is converted into millimeters per second using the conversion factor of 1 mm/s = 19.253 MHz.[38]

The spectrum of ScAgSn can be fitted to superpositions of two quadrupole doublets exactly in the 2:1 ratio predicted from the crystal structure. Table 4 compares the measured quadrupolar splitting with predictions from the WIEN2k calculation. In agreement with the experimental result, the calculation predicts a substantial difference in quadrupolar splitting between both tin sites. The numerical discrepancies between the calculated and the experimental values may be partly attributable to the low precision with which the quadrupole moment of the ^{119}Sn nuclear excited-state is actually known; in fact values ranging from 0.08 to 0.152 $\times 10^{-28}$ m^2 can be found in the literature.[39−41]

(37) Svane, A.; Christensen, N. E.; Rodriguez, C. O.; Methfessel, M. *Phys. Rev. B* **1997**, *55*, 12572.
(38) Stevens, J. G.; Stevens, V. E. *Mössbauer Effect Data Index*; Plenum: New York, **1975**; p 130.
(39) Boyle, A. J. F.; Bunbury, D. St. P.; Edwards, C. *Proc. Phys. Soc.* **1962**, *79*, 416−424.
(40) Niemeier, D.; Mehner, H.; Bismayer, U.; Becker, K. D. *Phys. Status Solidi b* **1999**, *211*, 581−593.
(41) Barone, G.; Silvestri, A.; Ruisi, G.; La Manna, G. *Chem.—Eur J.* **2005**, *11*, 6185−6191.

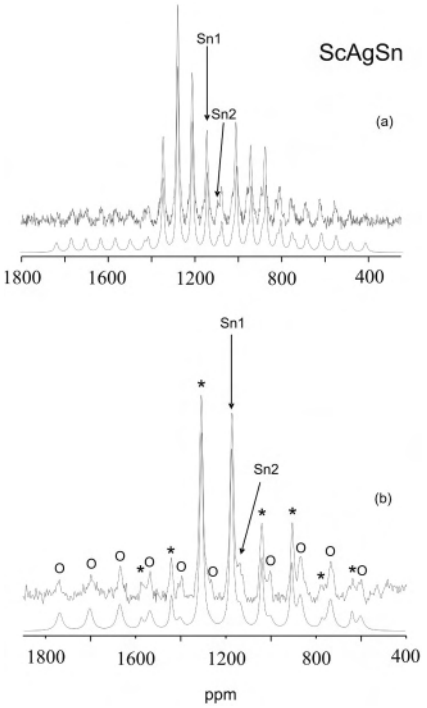

Figure 5. ^{119}Sn MAS NMR spectra for ScAgSn measured at room temperature: (a) spinning speed at 10 kHz and (b) spinning speed at 25 kHz. For each part of the figure, the top traces are the experimental spectra, while the bottom traces are simulations based on the chemical shielding parameters summarized in Table 5. Spinning sidebands are indicated with asterisks and circles for Sn(1) and Sn(2), respectively.

Table 5. ^{119}Sn MAS NMR Isotropic Magnetic Shielding ($\delta_{iso} \pm 2$ ppm) of ScAgSn Relative to Tetramethyltin[a]

400 MHz, 10 kHz					
tin site	δ_{iso}(^{119}Sn) (ppm)	η	δ_a (ppm)	Δ (Hz)	%
Sn1	1169	0.10	−383	1832	67
Sn2	1131	0.45	947	2727	33
500 MHz, 25 kHz					
tin site	δ_{iso}(^{119}Sn) (ppm)	η	δ_a (ppm)	Δ (Hz)	%
Sn1	1169	0.00	−388	1789	69
Sn2	1131	0.45	912	2673	31

[a] MAS centerband linewidths (FWHH) Δ ($\pm$10 ppm), magnetic shielding anisotropy ($\delta_A \pm 20$ ppm), and the asymmetry parameter ($\eta \pm 0.05$) extracted from the spectra using the DMFit routine are also given.

^{119}Sn and ^{45}Sc Solid-State NMR. Figure 5 shows the ^{119}Sn solid-state NMR spectra at two different spinning speeds. Consistent with the crystal structure, the spectra reveal two distinct spinning sideband manifolds in a 2:1 area ratio. Table 5 summarizes the magnetic shielding parameters extracted from these sideband manifolds using the DMFIT routine. Consistent with the information obtained from the Mössbauer spectra, the Sn1 majority site appears to have a higher local symmetry, featuring an approximately axially symmetric ^{119}Sn magnetic shielding tensor (with an asymmetry parameter η close to zero). In contrast, the Sn2 minority site is characterized by a significantly larger ^{119}Sn magnetic shielding anisotropy and an asymmetry parameter of 0.45. The effect of the structural distortion in relation to

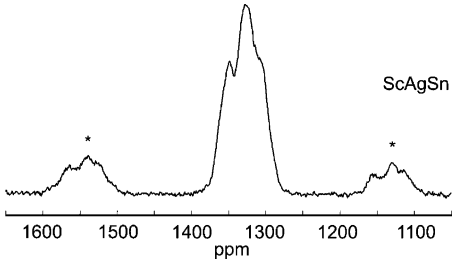

Figure 6. ^{45}Sc MAS NMR spectrum of ScAgSn measured at room temperature (spinning speed 25 kHz). Spinning sidebands are indicated with asterisks.

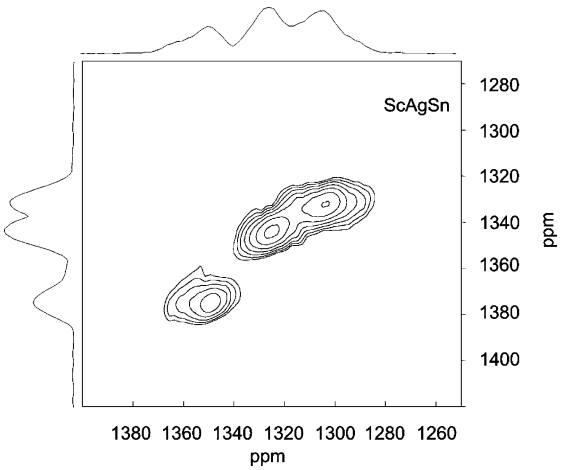

Figure 7. Sheared ^{45}Sc 3Q MAS NMR of ScAgSn measured at room temperature (spinning speed 25 kHz).

the parent structure of LuAgSn (top of the group subgroup scheme depicted in Figure 3), is clearly manifested in the solid-state NMR spectra: for the Sn1 site, the lowering of the local symmetry produces a significant increase in the shielding anisotropy in the superstructure, while for the Sn2 site the magnitude of the shift anisotropy is maintained, but a non-axial distortion becomes evident. Overall, the significant difference observed between Sn1 and Sn2 with regard to the ^{119}Sn shielding anisotropies is in good agreement with the significant difference observed in the calculated and experimental ^{119}Sn Mössbauer quadrupole splittings for these two sites.

Table 6. ^{45}Sc MAS NMR Isotropic Magnetic Shielding ($\delta_{iso} \pm 1$ ppm) of ScAgSn Relative to a 0.2M Aqueous Scandium Nitrate Solution[a]

site	δ_{iso}(^{45}Sc) (ppm)	η_Q(exptl)	η_Q(calcd)	C_Q(exptl) (MHz)	C_Q(calcd) (MHz)
Sc1	1367	0.82	0.90	8.8	8.9
Sc2	1336	0.91	0.96	7.2	7.0
Sc3	1322	0.72	0.71	9.5	9.8

[a] The electric field gradient asymmetry parameter ($\eta_Q \pm 0.05$) and nuclear electric quadrupole coupling constant ($C_Q \pm 0.2$ MHz) extracted from 2D slices in the TQ-MAS spectra using the DMFit routine are also given. These numbers are compared with the values calculated for the three Sc sites from the proposed crystal structure model, using the WIEN2K program.

The ^{45}Sc MAS NMR spectrum (Figure 6) shows a rather complex line shape, which might result either from the presence of multiple resonances, anisotropic broadening by second-order quadrupolar perturbations, or from a combination of both. The situation can be clarified by 2D triple-quantum MAS NMR correlation spectroscopy, which removes anisotropic broadening in one of the spectroscopic dimensions (F1). Indeed, the 2D spectrum shown in Figure 7, and its projection along the isotropic dimension clearly resolves the signals of three distinct scandium sites, in perfect agreement with the crystal structure model developed above. Because these ^{45}Sc NMR signals are well-separated in the 2-D contour plot, their anisotropic lineshapes can be well resolved, by plotting individual F1 "slices" along the F2 dimension. Figure 8 shows the individual subspectra thus obtained, along with the corresponding simulated spectra. For the Sc2 site in particular, significant line broadening is observed, reflecting a distribution of nuclear electric quadrupolar parameters. We attribute this effect to stress/strain effects in imperfectly crystallized samples, resulting in slight variations of the local environments. The nuclear electric quadrupolar coupling constant C_Q and the electric field gradient asymmetry parameter η_Q are summarized in Table 6, along with the corresponding values predicted from the

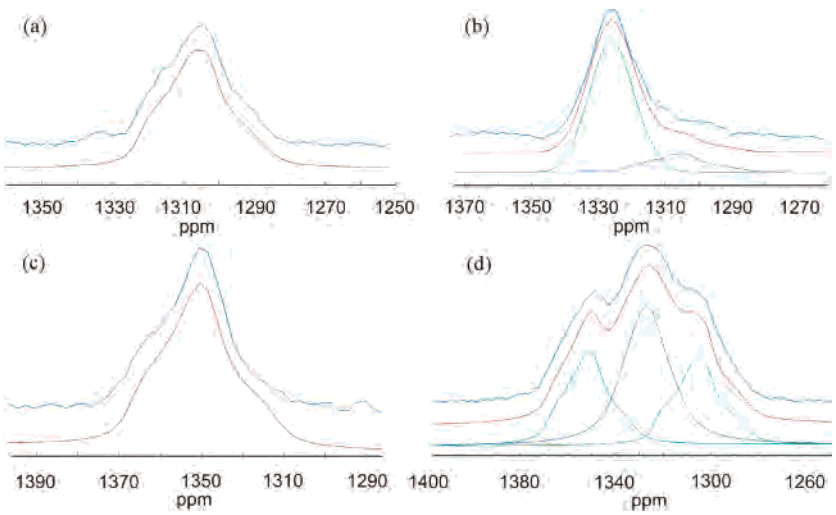

Figure 8. Spectral simulation of each ^{45}Sc site for the 1D spectrum taken the F2 row corresponding to the respective peak in the F1 dimension in 2D ^{45}Sc MQMAS, using the DMFIT package: (a) Sc3, (b) Sc2, (c) Sc1, and (d) spectral deconvolution of the regular 1D ^{45}Sc MAS NMR of crystalline ScAgSn, using the spectral line-shape simulated with the parameters summarized in Table 6.

suggested crystal structure using the WIEN2k program. Overall, the *near-perfect* agreement between the experimental and the predicted electric field gradient parameters provides strong support for the crystal structure model developed above and suggests the NMR peak assignments depicted in the Table. On the basis of these line shape parameters, the one-dimensional ^{45}Sc MAS NMR spectrum can be simulated, which is found to be in excellent agreement with the experimental data (see Figure 8d).

Conclusions

Within the REAgSn series, a variety of crystal structures can be adoped. Of these materials, ScAgSn, the representative with the smallest rare earth cation, forms a crystal structure that can be derived from the parent ZrNiAl structure formed by its homologs TmAgSn and LuAgSn; however, rare earth cation size mismatch effects produce local distortions that result in superstructure formation. A structure solution from imperfect (tripled) crystals proved only possible on the basis of important constraints provided by state-of-the-art solid-state NMR and Mössbauer spectroscopy. In particular, the present results underline the utility of high-resolution ^{45}Sc MAS NMR as a new probe of the structural chemistry of rare earth intermetallic compounds.

Acknowledgment. We are grateful to Dipl.-Ing. U. Ch. Rodewald for the intensity data collection and to H.-J. Göcke for the work on the scanning electron microscope. This work was supported by the Deutsche Forschungsgemeinschaft. C.P.S. is indebted to the NRW Graduate School of Chemistry for a doctoral fellowship stipend.

Supporting Information Available: Crystallographic data in CIF format. This material is available free of charge via the Internet at http://pubs.acs.org.

IC061691O